Power flow and reliability analysis of a non-isolated PV/grid connected quasi resonant converter for off-board EV charging station

Harini S[a], Chellammal N[a] and Ramesh C Bansal [b,c]

[a]Department of Electrical and Electronics Engineering, College of Engineering and Technology, SRM Institute of Science and Technology, Kattankulathur, Chennai, India; [b]Department of Electrical Engineering, University of Sharjah, Sharjah, United Arab Emirates; [c]Department of Electric, Electronic and Computer Engineering, University of Pretoria, Pretoria, South Africa

ABSTRACT

Growing awareness of greenhouse gas emissions and exhaustion of fossil fuels leads to the adoption of electric vehicles (EVs). However, the major limitations with respect to EV technology are the driving range and charging time. Also, the proliferation of EVs overloads the power grid and paves the way of incorporating renewable energy sources and energy storage devices. The use of multiple sources necessitates the deployment of compact, low-cost, and high-power electronic converters. This paper proposes a novel configuration of a Multi-Source Non-Isolated Quasi-Resonant Converter (MSNQRC) to overcome the limitations in the charging infrastructure. Due to the presence of a quasi-resonant network, the proposed MSNQRC with a single switch can achieve high voltage gain even at low-duty cycles, provide continuous current and low voltage stress. In addition, this paper elaborates on the parametric design of the converter along with PV modeling based on load ratings and the reliability research of MSNQRC by analysing component failures. A prototype model of 300W is built to verify the efficacy of the designed converter model. The results thus obtained validate the designed model and prove that the proposed system can be used for off-board battery charging systems.

KEYWORDS

Battery; DC-DC boost converters; electric vehicle charger; photovoltaic system

1. Introduction

Hybridization of photovoltaic (PV) modules, grid, and battery storage packs has found its way in different commercial applications. Hybrid systems are mainly utilized in electric vehicles, energy storage systems, and in many industrial applications. Renewable sources like solar energy are readily available and economic [1]. As referred in reference [2], there exist certain challenges during the integration of DC bus system, and different components such as loads and energy storage devices. To overcome the challenges and maximize the performance of grid, solar arrays, electric vehicles (EVs), and loads connected to DC buses, suitable controllers must be developed. The importance of power management system (PMS) of an EV in a hybrid PV/grid multi-source power supply is elaborated in [3,4].

EV chargers with hybrid systems are implemented in commercial places to charge electric cars while parked during the daytime. Maximum PV energy consumption for EV charging with minimal grid energy exchange is the objective of a hybrid system. The features of EV – PV charger will be:

- Development of sustainable charging stations.
- Reduction of grid dependency with an increase in the utilization of renewable energy.
- Clean, renewable, cost-effective, and easily available alternative energy source requirement during the non-availability of grid power [5–8].

Reference [9] discusses the planning methodology for an Electric vehicle charging station (EVCS) with optimization techniques, and sensitivity analysis. Also, researchers [10] provide an assessment of EVCS location and its impact on the local distribution network [11]. A comprehensive analysis of EVCS, including the choice of locations, sizing methods, modeling, charging methodologies, and modes of transport, is well elaborated in [12]. Paper [13] examined bidirectional converters for rapid charging EV/PHEVs. The authors concluded that high gain and efficiency converter is suitable to charge the high rated battery. Reference [14] discusses the performance of low voltage battery packs, maintenance, safety, and compares three battery pack voltages (24 V, 48 V, and 300 V). The article [15] suggested

CONTACT Chellammal N chellavenkat09@gmail.com; Ramesh C Bansal rcbansal@ieee.org Department of Electrical and Electronics Engineering, College of Engineering and Technology, SRM Institute of Science and Technology, Kattankulathur, Chennai, Tamilnadu 603203, India

semi-bridgeless ac-dc converters at the front end for rapid charging with 400 V dc voltage to overcome North America's low residential power (Level 1/ level 2). Grid-assisted bidirectional EV charging for PHEVs was presented in [16]. The study in [17] examined wireless EV charging technologies and power electronics (PE) designs. The paper [18] proposes a Constant Current Constant Voltage (CCCV) charging method for grid-connected EVs with voltage-control management. A novel resonant converter topology for charging EVs is proposed using a CCCV profile with experimental results [19]. The study in [20] covers the pulse charging method for Li-Ion battery charger, CCCV with linear and switching circuits. In [21], a charging system for electric vehicles (EVs) employing distributed energy resources (DERs) such as PV array and a battery storage system is analysed. This study also presented charging EVs with a distinct charging profile (CC charging profiling), as well as a small-scale power system for a single EV [22]. The authors of [23,24] discussed the design of a PV system for charging EVs with BESS.

The purpose of PV-powered EVCS is to improve the benefits of utilizing renewable sources, and to reduce the costs associated with charging, and dependency on the grid. On the other hand, with the help of a comprehensive power infrastructure, it is essential to develop a CCCV charging profile that is both efficient and safe. Table 1 provides a comparative study of EVCS. In recent years, a significant amount of research has been devoted to evaluating the reliability performance of power equipped converters [25,26]. The power electronic converter's reliability is examined based on switch type, application, and redundant structure in [27–29]. The reliability of a 3-phase interleaved boost converter can be enhanced using soft switching without auxiliary components [30]. The number of stages that can be modified in an optimization model for an interleaved boost converter is presented in [31]. This approach achieves a compromise between both affordability and reliability. In [32], a comparison of reliability levels of interleaved and single-stage boost converters' is presented. The two-stage interleaved boost converter that operates at half the energy provides the maximum level of reliability, and it needs more components than a single-stage model. The life time of an isolated converter with a redundant power source application is characterized in [33] by voltage, current stress, ambient temperatures, junction temperatures, load profiles, switching and conduction losses, and load profiles. This paper describes a MSNQRC interfaced to off board EVCS. The PV array, grid, and EV batteries can exchange energy in all possible ways. DC-DC converters are synthesized, and parameters are designed for EVCS. Voltage control mode and current control mode are incorporated to charge vehicles with the utmost efficiency in the shortest period of time possible.

The proposed charging method is validated via simulation in a variety of operational scenarios. With this intention, description of the system of EVCS and modeling of PV is described in Section 2. The considerations in the parametric design of a power source, ratings, operating principle, and modes of operation of MSNQRC are presented in Sections 3 and 4, respectively. Designing a controller for an EV battery charging is discussed in Section 5. Prototype of MSNQRC is realized, and the experimental results are presented in Section 6 to validate the theoretical and simulation-based analyses. The dynamic behavior of the converter is described in Section 7. In the final Section 8, the conclusions are summarized.

2. Description of the system

2.1. Configuration of a system with an EV connected to dc bus

As illustrated in Figure 1, the system uses a grid as the primary power source and PV as the secondary source. A secondary energy source is needed to balance the power demand when one input source fails

Table 1. Comparative study on EVCS.

Ref.	Design for charging EVs	Modes	Configuration of system	Efficiency	Voltage regulation	Charging hour taken	Method of Charging
[2]	Detail study for 3 EV's battery (load)	3	Grid connected	Not mentioned	Good	<3 hr	CCM and CVM
[20]	Detail study for 1 EV's battery (load)	3	Standalone	Not mentioned	Worst	Not mention	Stepped-CC
[22]	Detail study for 5 EV's battery (load)	Nil	Grid connected	Not mentioned	Not mentioned	4–5 hr	CC
Proposed method	Detail study for 10 EV's battery (load)	3	Grid/PV connected	Calculated >91% (CEC)	Excellent	4 hr	CC-CV

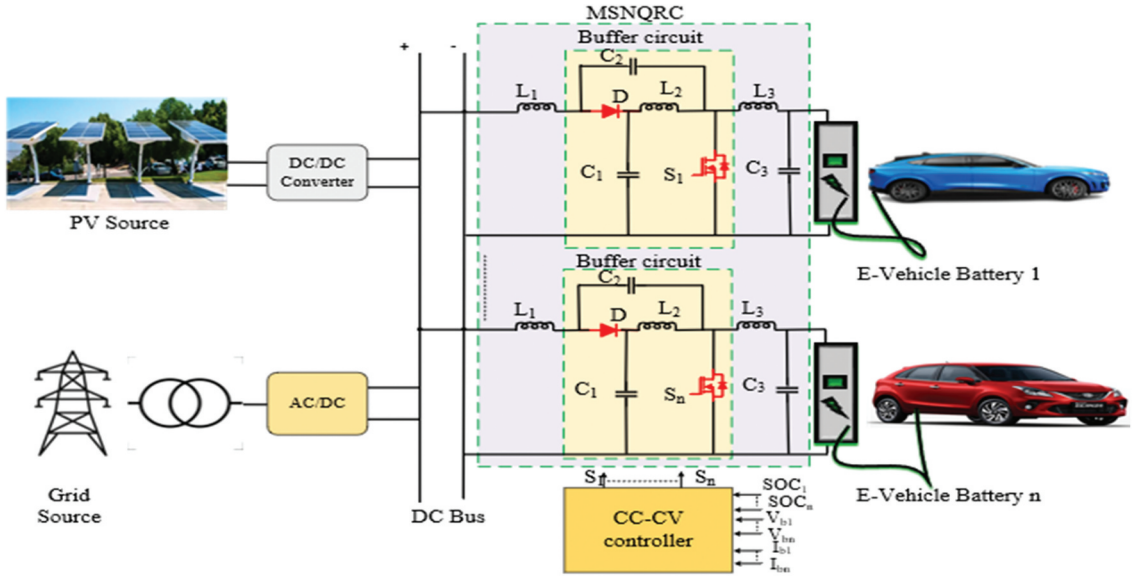

Figure 1. Schematic architecture for off board EVs charging station.

to charge the electric vehicle. During the daytime, the PV source can meet the load demand. Likewise, when the grid is unable to meet the load demand, the PV source supports the required EV power. According to CC-CV control system, grid/PV interfaced MSNQRC is used to supply power from the utility grid to the battery. Ten charging sockets, points, or outlets on the load side are intended to use MSNQRC to charge EVs at various voltage levels. Electric vehicle battery voltages are often multiples of 24 V and 48 V.

2.2. Modelling of PV array

The photovoltaic module serves as the interface for converting light energy into electrical energy. To model this device, it is necessary to utilize the irradiance and temperature of the surrounding environment as input variables. Output can be current, voltage, or power. It is essential to utilize an appropriate PV module. A particularly precise mathematical model [21] that is ideal for circuit modeling is the one depicted in Figure 2(a). The mathematical model of PV can be deduced from Equations (1–5).

$$I_{PV} = I_{Ph} - I_d - I_{sh} \tag{1}$$

$$V_{PV} = V_d - R_S I_{PV} \tag{2}$$

$$I_{PV} = I_d - \frac{V_{PV}}{R_{Sh}} - I_{PV} = 0 \tag{3}$$

$$I_d = I_o\left(e^{\frac{V_{PV}}{V_T}} - 1\right) \tag{4}$$

$$I_{Ph} = [I_{sc} + K_i(T - 298)] * \frac{G}{1000} \tag{5}$$

The temperature coefficient of cell's short circuit current, denoted as K_i, is 0.0017 Amp/C. In the above equations, I_{sc} represents the short circuit current of the cell in amperes (A), and G represents the solar radiation in watts per square meter (W/m^2). The impact of temperature fluctuations and wind velocity is neglected.

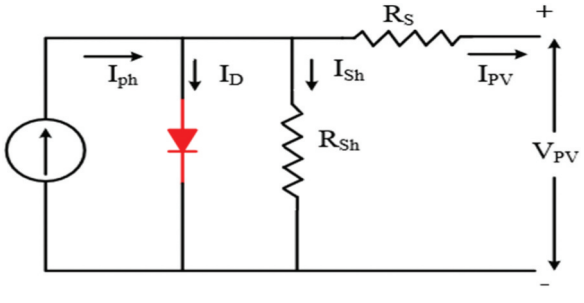

Figure 2a. Schematic diagram of MSNQRC modelling circuit.

2.3. Modeling of MSNQRC

Figure 2(b) depicts the schematic diagram of MSNQRC modeling circuit, with two sources, PV, and grid, and the load side is accommodated with an EV battery.

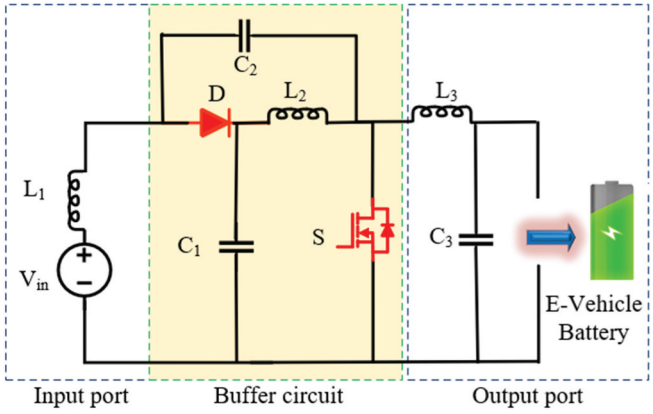

Figure 2b. Schematic diagram of QRC.

High gain DC-DC converters are required for PV and MSNQRC works in boosting mode to provide high gain during charging. While designing parameters for MSNQRC in boost mode, the input voltage ($V_{input\text{-}min}$ and $V_{input\text{-}max}$), nominal output voltage, and maximum output current is required to compute the power stage.

3. Ratings and parametric design of PV module, and QRC

3.1. Load estimation

The MSNQRC system consists of specific 10 EV battery packs of 28 V, 8Ah and 48 V, 12Ah as load in parallel. The overall power capacity of the load may be computed as indicated below in Equation (6):

$$P_{10EV} = (5 * 24 * 8) + (5 * 48 * 12) = 3.840kW \quad (6)$$

3.2. Sizing of PV system

PV modules are designed to charge 10 electric vehicles simultaneously. In addition, the PV modules are designed to recharge the EV battery during daytime without moving the vehicles. The EVs charge for 4 hours, from 0% to 100% SOC in the worst-case scenario, to reduce grid dependency and improve the utilization of PV source. Charging time is decreased by increasing the number of PV modules by increasing the installation of PV. PV is included with the grid to attain high power and fast charging. The PV module's power to charge the 10 batteries is estimated by Equation (7).

$$P_{PV} = \frac{P_{10EV}}{T_{Ch} * \eta_{MNSQRC} * \eta_{PV}} = \frac{3.840}{4 * 0.9 * 0.92} = 1.159\text{kW} \quad (7)$$

where T_{ch} is the time required for charging, η_{PV} is the efficiency of the PV converter, and η_{MSNQRC} is the MSNQRC efficiency. For PV modules rated at 20W, the number of PV modules (Npv) for 10 battery-powered EVs is calculated as shown in Equation (8).

$$N_{PV} = \frac{P_{PV}}{P_{PVm}} = \frac{1.159}{0.020} = 58 \text{ modules} \quad (8)$$

So, 58 PV modules are needed to be connected in parallel at a rated voltage of 12 V and a rated current of 1.6A for 10 EV's batteries.

3.3. Inductor

The inductor current ripple is essential for designing inductors. Equation (9) represents the inductor current ripple. Inductor voltage $V_{L1} = L(di/dt)$ into account.

$$\Delta I_{L1} = \frac{V_{in}(1-d)}{(1-2D)f_s L_{1g}} \quad (9)$$

Inductors are designed to limit twice the magnitude of the ripple current differential. The inductor current i_{L1} should oscillate within 20% of average current. Equation (10)helps to design inductor L_1 by utilizing the appropriate current ripple and volt-sec balancing theory.

$$L_1 = \frac{R(1-2d)}{x_{L1}\%f_s d} \quad (10)$$

where f_s represents switching frequency.

Similarly, inductor values for L_2 and L_3 are designed as mentioned by Equation (11).

$$L_2 or L_3 = \frac{R(1-2d)}{x_{L2,3}\%f_s d} \quad (11)$$

3.4. Capacitor

The capacitors are designed to limit the change in voltage difference (ΔV_C) as mentioned by Equation (12). By assumption, it is designed with the permissible value of ΔV_{C1} as 20% of the average capacitor voltage.

$$\Delta V_{C1} = \frac{V_{in}(1-d)d}{R(1-2d)^2 f_s C_1} \tag{12}$$

Using capacitor voltage charge-sec balance and voltage ripple, the capacitor C_1 is designed as shown in Equation (13).

$$C_1 = \frac{d}{x_{C1}\%R(1-2d)f_s D} \tag{13}$$

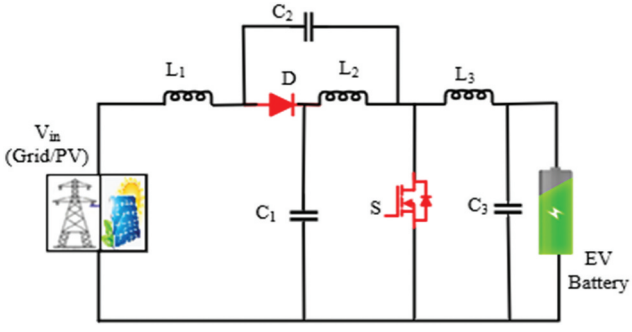

Figure 3. Power circuit for MSNQRC.

The C_2 and C_3 capacitor values are designed as represented by Equation (14).

$$C_2(or)C_3 = \frac{d}{x_{C1}\%R(1-2d)f_s D} \tag{14}$$

4. Description, operating principles, and modes of operation of MSNQRC

Figure 3 depicts the designed power circuit for MSNQRC. This circuit contains one power-controlled switch (S), three (C_1, C_2, and C_3) capacitors, and three (L_1, L_2, and L_3) inductors, in addition to one uncontrolled switch (D). The controlled power switch S transfers power from the grid (primary source) and PV (secondary source) to EV battery (load) based on demand. Consequently, the grid and the photovoltaic panel are regarded as input ports, whereas the EV battery is connected at the output port.

Depending on the availability of supply and the switching conditions of switch S, the proposed MNQRC has three operating modes with two dissimilar states. Figure 4 depicts different modes of operation and the equivalent circuits for each interval of MSNQRC operating period. Table 2 provides details regarding the ports involved and the direction of power transfer in MSNQRC during various modes of operation. Switches, diodes, inductors, and capacitors are assumed to be lossless components.

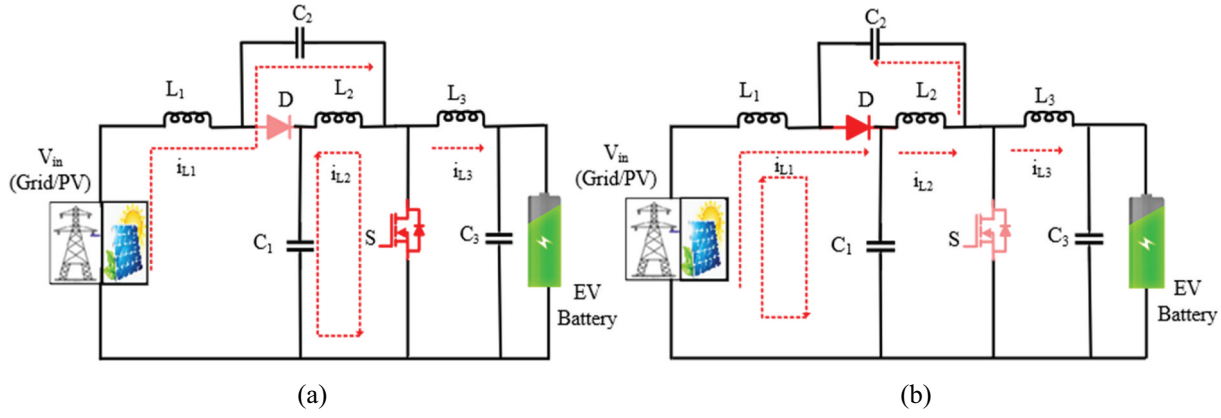

Figure 4. Operation of MSNQRC, (a) switch S = ON, (b) switch S = OFF.

Table 2. Operating modes of proposed MSNQRC.

Mode	Power flow direction	Type of Mode	Constraints
Mode-1	Figure 5(a) Grid to EV battery	SISO-Single Input Single Output	• Grid power is sufficient. (P_{grid}>P_{bat})
Mode-2	Figure 5(b) PV to EV battery	SISO-Single Input Single Output	• PV power is sufficient. (P_{PV}>P_{bat})
Mode-3	Figure 5(c) Grid and PV to EV battery	MISO-Multiple Input Single Output	• Grid + PV is sufficient. ((P_{grid}+P_{Pv}) >P_{bat})

4.1. Operating principle

4.1.1. STATE 1

During this interval $0<d_1T_S$, the switch S is turned on as depicted in Figure 4(a). The current I_{L1} flowing through the inductor L_1 increases with a positive slope. The discharge of capacitor C_2 magnetizes the inductor L_2 and charges the capacitor C_1. As a result, the inductor L_3 and capacitor C_2 are discharging. Equations (15–18) are valid for operation in state 1.

$$V_{L1} = V_g + V_{C2} \tag{15}$$

$$V_{L2} = V_{C1} \tag{16}$$

$$V_{L3} = -V_{C3} \tag{17}$$

$$V_{C3} = V_O \tag{18}$$

4.1.2. STATE 2

During this period, $d_1Ts<t<Ts$ switch S is turned off as shown in Figure 4(b). As a result, there is a drop in inductor current i_{L1g} with a negative slope. The inductor L_2 and the capacitor C_1 are discharging. L_3 and C_2 are charged. The steady state equations related to the state are described as shown in Equations (19–22).

$$V_{L1} = V_g - V_{C1} \tag{19}$$

$$V_{L2} = -V_{C2} \tag{20}$$

$$V_{C1} - V_{L2} - V_{L3} - V_{C3} = 0 \tag{21}$$

$$V_{C3} = V_{C1} - V_{L2} - V_{L3} \tag{22}$$

The volt-second balance Equations (15–24) with respect to inductor 'L' and charge-second balance equation with respect to capacitor 'C' can be used to calculate the capacitor's voltages and voltage gain using Equations (23–26).

$$\mathrm{V_{C1}} = \frac{(1-\mathrm{d_1})\mathrm{V_{in1}}}{(1-2\mathrm{d_1})} \tag{23}$$

$$V_{C2} = \frac{d_1 V_{in1}}{(1-2d_1)} \tag{24}$$

$$GainG = \frac{(1-d_1)}{(1-2d_1)} \tag{25}$$

$$V_{bat} = \frac{(1-d_1)V_g}{(1-2d_1)} \tag{26}$$

4.2. Modes of operation

4.2.1. Mode 1 ($P_g > P_{PV}$) single input single output

Figure 5(a) depicts the equivalent circuit of MSNQRC as well as the power flow schematic while the converter is

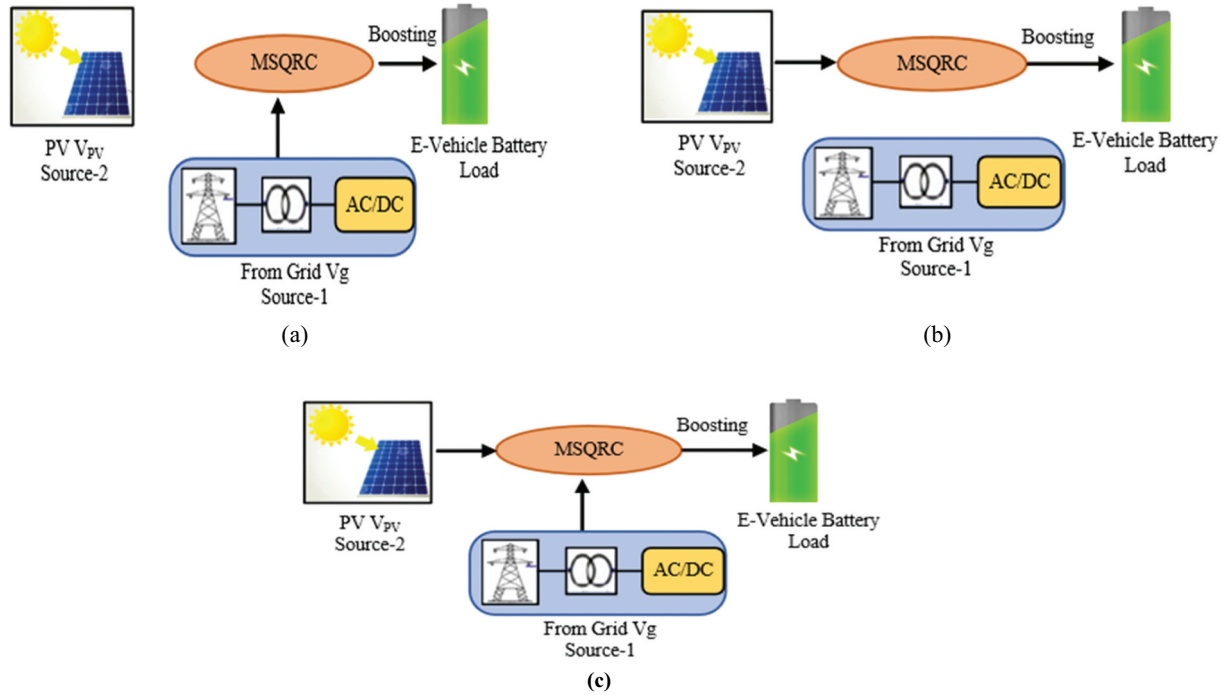

Figure 5. Modes of power transfer, (a) mode-1 (SISO).

operating in mode-1. During such conditions, the grid delivers power individually to EV

$$Pg > P_{PV}$$

4.2.2. Mode 2 -(P_{PV}>P_g) single input single output

During the daytime PV provides sufficient power to meet the load demand. This mode delivers energy from the PV to EV batteries individually, as depicted in Figure 5(b).

$$P_{PV} > P_g$$

Grid to EV's Battery, (b) Mode-2 (SISO) PV to EV's Battery, (c) Mode-3 (DISO) Grid/PV to EV's Battery.

4.2.3. Mode 3 - ($P_{PV} = P_g$) multiple input single output

When the demand for EV battery power is significant, as depicted in Figure 5(c), both PV and the grid provide power to the EV battery. During this state, the switch 'S' is activated.

$$P_g = P_{PV}$$

5. Control design for MSNQRC

5.1. EV battery charging controller

Charge controllers regulate the rate at which voltage and current are delivered to a vehicle's battery. It protects the battery from overcharging. The controller is responsible for controlling the switching sequence of the power electronic interface. Figure 6 depicts the conventional PI controller used to control the output voltage and current of MSNQRC. Using constant-voltage and constant-current controllers, the EV battery is charged efficiently. Figure 7 demonstrates that for rapid charging, both the

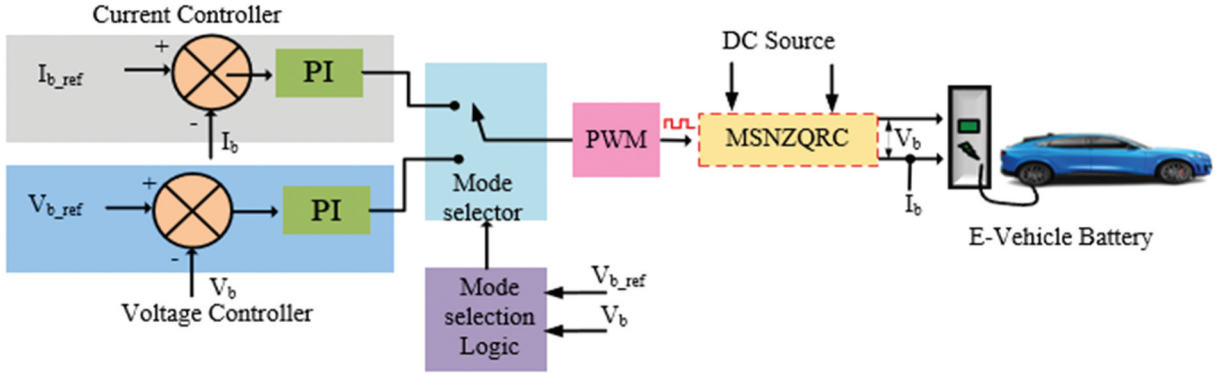

Figure 6. CC-CV EV battery charging controller.

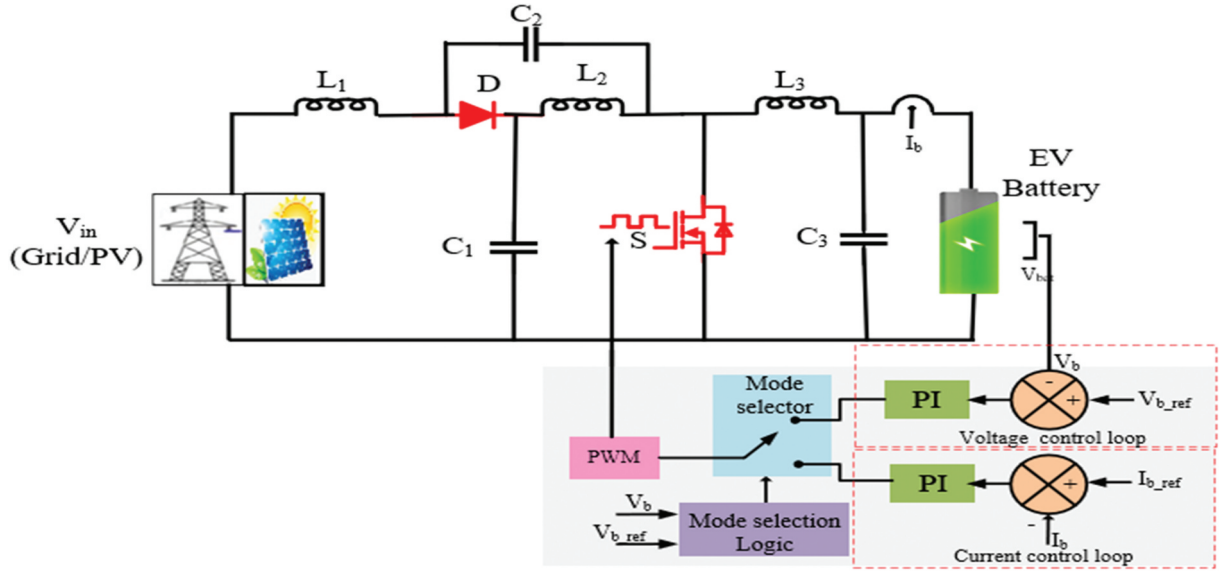

Figure 7. Equivalent circuit of MSNQRC with control.

inner current control loop and the outer voltage control loop used for constant voltage and constant current charging are employed. Proportional-Integral control algorithm is used to modulate EV battery charging. The most popular PI controller is designed to eliminate the steady state error and regulate the battery current and voltage. Using Ziegler-Nichols tuning method, the proportional gain (K_p) and integral (K_i) with time T_i values are determined from Equations (27 and 28).

$$P_{out} = K_p e(t), I_{out} + K_i \int_0^t e(t)dt \tag{27}$$

$$PI_{Controller} = K_p\left(1 + \frac{1}{T_i S}\right), K_p = 0.9\frac{T}{L}, T_i = \frac{L}{0.3} \tag{28}$$

6. Power losses and reliability analysis of MSNQRC

6.1. Power loss Analysis

Parasitic resistances are described for the effective analysis of the switch in MSNQRC. r_s represents the ON-state resistance of switch (S), r_D, and V_D represent forward resistance, and threshold voltages of diode D respectively. Total power losses (P_S) of the switch are estimated for the assumed 40% duty cycle and 10 V input voltage. The total switch power loss (P_S) is calculated using Equation (29).

$$P_S = P_{r_s} + \frac{P_{SL}}{2} \tag{29}$$

Switch power conduction loss (P_{rs}) is evaluated using Equation (30).

$$P_{r_s} = r_S I_S^2 = r_S\left(\frac{dI_o}{(1-2d)}\right)^2 \tag{30}$$

'Io' and 'd' are the output current and duty cycle of MSNQRC switch, respectively.

MSNQRC switching loss (P_{SL}) is

$$P_{SL} = f_S C_S\left(\frac{V_{in}}{(1-d)}\right)^2 \tag{31}$$

V_{in}, C_S, and f_s are the input voltage, snubber capacitor, and switching frequency, respectively. Substituting the Equations (30) and (31) in (29).

$$P_S = 1.02W \tag{32}$$

Equation (32) determines diode D (P_D) power loss.

$$P_D = P_{FRD} + P_{FVD} \tag{33}$$

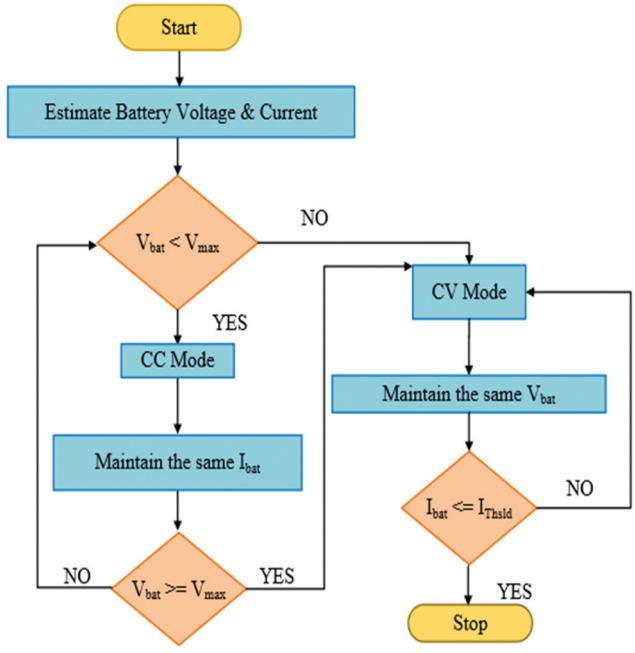

Figure 8. EV battery charging controller.

The forward resistance loss (P_{FRD}) of diode D can be calculated using the Equations (34-35)

$$P_{FRD} = r_D {I_D}^2 = r_D\left(\frac{I_o}{(1-2d)}\right)^2 \tag{34}$$

where r_D and I_D represent the diode's resistance and current flow, respectively. The forward voltage loss (P_{FVD}) of diode D can be calculated as follows:

$$P_{FVD} = V_D I_D \tag{35}$$

Substitute Equations (34) and (35) in (33), then the diode power loss P_D is

$$P_D = 0.508W \tag{36}$$

Here, closed-loop voltage mode and current mode control using a PI controller with variable input and constant output has been implemented. Figure 8 illustrates the flowchart for EV battery charging method (constant voltage and constant current).

6.2. Reliability estimation

In this section, the evaluation of the reliability of an MSNQRC based on MILHDBK-217F [34] without any variation in component characteristic parameters is presented.

Table 3 contains the list of design elements. Under the assumption of a constant failure rate λ_{SYSTEM}, the system's reliability can be calculated as shown in Equation (37).

Table 3. Parameter details of MSNQRC.

Parameter used	Input Voltage V_{in}	Inductors L_1, L_2, L_3	Capacitor C_1, C_2, C_3	Battery Rating	Switching Frequency f_s
Simulation	Mode 1–12 V (V_{in1}) Mode 2–12 V (V_{in2}) Mode 3–10 V (V_{in1}) and 10 V (V_{in2})	10 mH	12.6μF, 12.6 μF, 100 μF	24 V, 10 Ah	20 kHz
Experimental	Mode 1–12 V (V_{in1}) Mode 2–12 V (V_{in2}) Mode 3–10 V (V_{in1}) and 10 V (V_{in2})	12 mH	10 μF, 10 μF, 100 μF	24 V, 10 Ah	MOSFET (IRFP4227Pbfx2 r_s = 15 mΩ, C_S = 46 PF-20 kHz), DIODE (RF1001NS2DFH) r_D = 20 mΩ, V_D = 0.87mV

$$Rs(t) = e^{-(\lambda SYSTEM \times t)} \tag{37}$$

$R_S(t)$ is the probability of no failure occurring during the time interval 't'. λ_{SYSTEM} displays the system failure rate (failure per hour). Using the reliability probability formula in Equation (38), the mean time to failure (MTTF) of MSNQRC can be calculated.

$$MTTF = \int_0^\infty Rs(t)dt = \frac{1}{\lambda_{SYSTEM}} \tag{38}$$

The failure rate of power MOSFETs (failure per hour) can be expressed using Equation (39)

$$\lambda_{MOSFET} = \lambda_B \pi_E \pi_T \pi_A \pi_Q \tag{39}$$

The base failure rate (λ_B) is 0.012, both the quality factor (π_Q) and the application factor (π_A) are 8. The environmental factor π_E for MSNQRC in electric vehicle charging station is 9. Equation (40) determines the junction temperature and temperature factor.

$$\pi_T = exp\left[-1925\left(\frac{1}{T_J+273} - \frac{1}{298}\right)\right]$$
$$(where\ \pi_T = temperature\ factor) \quad T_J = T_a + (\theta_{JA})\ P_{sw} \tag{40}$$

For MOSFET packaging in D2PAK, set junction-to-ambient thermal resistance θ_{JA} is 18 C/W and ambient temperature T_a is 25° Celsius. The P_{SW} represents the switching device's total power loss (the sum of conduction and switching losses). The MOSFET failure rate can be computed from previously obtained parameters using Equation (41).

$$\lambda_{MOSFET} = \lambda_B \pi_E \pi_T \pi_A \pi_Q = \pi_T \times 6.912 \tag{41}$$

Considering the power loss in a switch as 1.308 W (which includes conduction and switching losses), Equation (42) determines the MOSFET failure rate. where TJ is 48.544.

$$T_J = T_a + (\theta_{JA})P_{sw} = 25 + (18 \times 1.308)$$
$$\pi T = exp[-1925\left(\tfrac{1}{T_J+273} - \tfrac{1}{298}\right)] \tag{42}$$
$$\lambda_{MOSFET} = 11.09$$

Similar analyses can be implemented on MSNQRC diode, inductor, and capacitor. The failure rate and MTTF of MSNQRC are represented by Equations (43) and (44), respectively, for the MSNQRC under consideration.

$$\begin{aligned}\lambda_{SYSTEM} &= \lambda_{MOSFET} + \lambda_{CAP} + \lambda_{DIODE} + \lambda_{Inductor} \\ &= \lambda_{SYSTEM} 6.912 X exp\left[192\left(\frac{1}{Ta + (\theta JA)Psw + 273} - \frac{1}{298}\right)\right] \\ &+ 120\left(0.0028\left[\left(\frac{Sc}{0.55}\right)^3 + 1\right] X exp\left[4.09\left(\frac{T+273}{358}\right)^{5.9}\right]\right) \\ &X0.495621 + 0.0116 X exp\left[-3091\left(\frac{1}{Ta+(\theta JA)Pd+273} - \frac{1}{298}\right)\right] \\ &+ 0.0108 X exp\left[\frac{0.11}{8.617x10 - 5}\left(\frac{1}{THS+273} - \frac{1}{298}\right)\right] \\ \lambda_{SYSTEM} &= 12.16 failure/millionhours\end{aligned} \tag{43}$$

$$\text{MTTF} = \frac{1}{\lambda\ \text{SYSTEM}} = \frac{106}{\lambda\ \text{SYSTEM}} \text{hours/failure}$$
$$= 9.38 \text{year/failure} \tag{44}$$

Figure 9 and Table 4 show the fluctuations in reliability with respect to MSNQRC parameters, including gain, output voltage, power losses, duty cycle, and duration.

7. Results and discussion

As shown in Figure 10, to charge an EV battery with a capacity of 56.6 kWh, 650 V, 83.3Ah, the selection of the converter switch should have the rating of 650 V C6D Silicon Carbide Schottky Diodes

Table 4. Analysis of MI-QRC with various duty cycles.

Duty	Gain	Operating Time	Power loss	λ_{sw}	MTTF year/Failure (MOSFET)
0.1	1.12	0.5 x 10–5	0.0066	6.93	16.473
0.2	1.33	1 x 10–5	0.0342	7.005	16.29
0.3	1.75	1.5 x 10–5	0.944	9.7	11.65
0.4	3	2 x10–5	1.522	11.09	9.38
0.45	5.5	2.25 x10–5	2.712	17.16	6.65

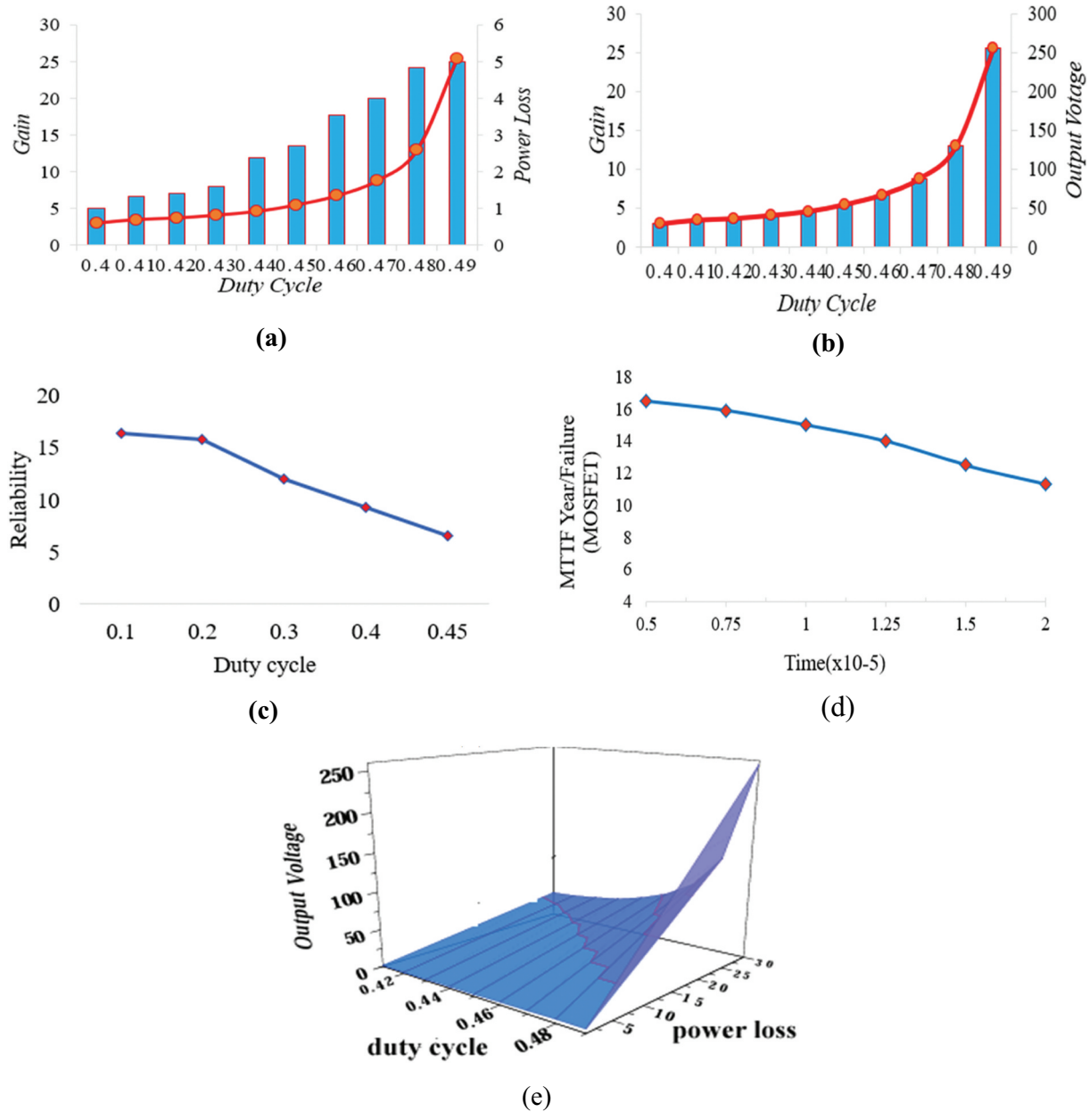

Figure 9. (a) Gain and power losses for various duty cycles, (b) gain and output voltage for various duty cycles (c) reliability with duty cycle (d) MTTF with respect to time. (e) output voltage, duty cycle and power losses.

(C6D20065D) when 'D' is varied from 0.1 to 0.49 for an input voltage.

In the laboratory, a 300 W, 20 kHz MSNQRC with MOSFET switches is built with the designed values and are listed in Table 3. The MSNQRC employs two DC power sources. To sustain battery voltage, a simple PI controller [28] is used. The Xilinx FPGA Spartan 6 generates control signals that are applied to trigger the MOSFET. A 20 kHz switching frequency is used for gate pulses. As previously stated, the MSNQRC is capable of charging EV batteries at low duty cycles.

Validation of efficiency and high voltage gain of MSNQRC at 0.4 duty cycle and constant input voltage are tested experimentally as a proof of concept. Experiments were carried out with MSNQRC with a 12 V voltage source. Duty ratios of 40% to 49% were chosen for boost operations, with a gain

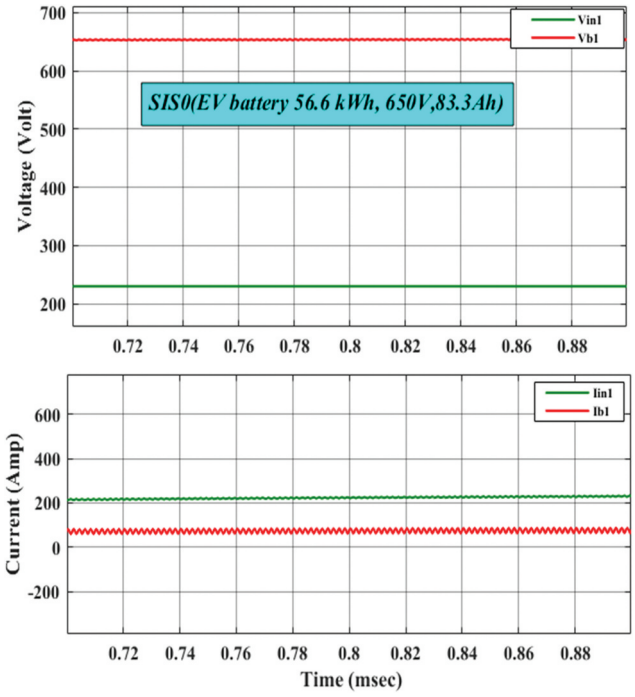

Figure 10. Simulation results of MSNQRC for SISO mode to charge an EV battery of capacity 56.6 kWh, 650V, 83.3Ah.

increasing up to 23 times. Figures 11 and 12 show the simulation, and experimental output of all three modes of operation for the voltage source and current, load current, and voltage. Furthermore, the test is carried out with a 12 V source voltage (grid and PV) and the load voltage (battery voltage) as 24 V. Figure 13 shows the inductor current for all three modes and Figure 14(a–c) shows the experimental output of inductor current for all three modes.

Figure 15 shows the behavior of MSNQRC during a dynamic change in the input voltage. For an open loop system, the MSNQRC provides quick transient performance. For an instance, when the source voltage is increased from 10 V to 12 V, a change in output voltage is observed from 27.7 to 28.1 V as shown in Figure 15(a) for mode 1. An increase in the input voltage of 10 to 12 V, causes a change in output voltage from 27.6 to 28.2 V as shown in Figure 15(b) for mode 2 and during mode 3 when input voltage is increased from 10 to 12 V, there was a change in output voltage from 27.75 to 28.3 V as shown in Figure 15(c). The regulated duty ratio of switch S with the EV battery charging controller manages

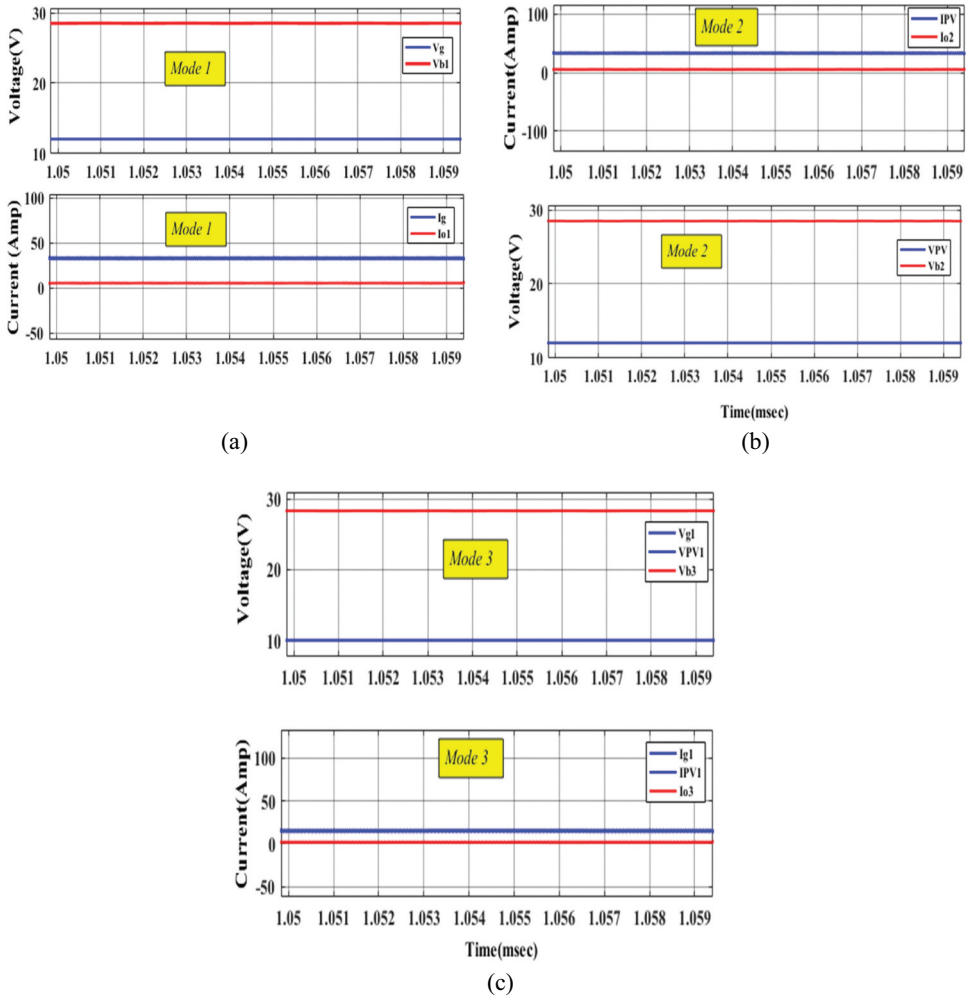

Figure 11. Simulation results, (a) mode-1 grid (source) to EV battery (load), (b) mode-2 PV (source) to EV battery(load), (c) mode-3 both grid and PV (sources) to EV battery (load).

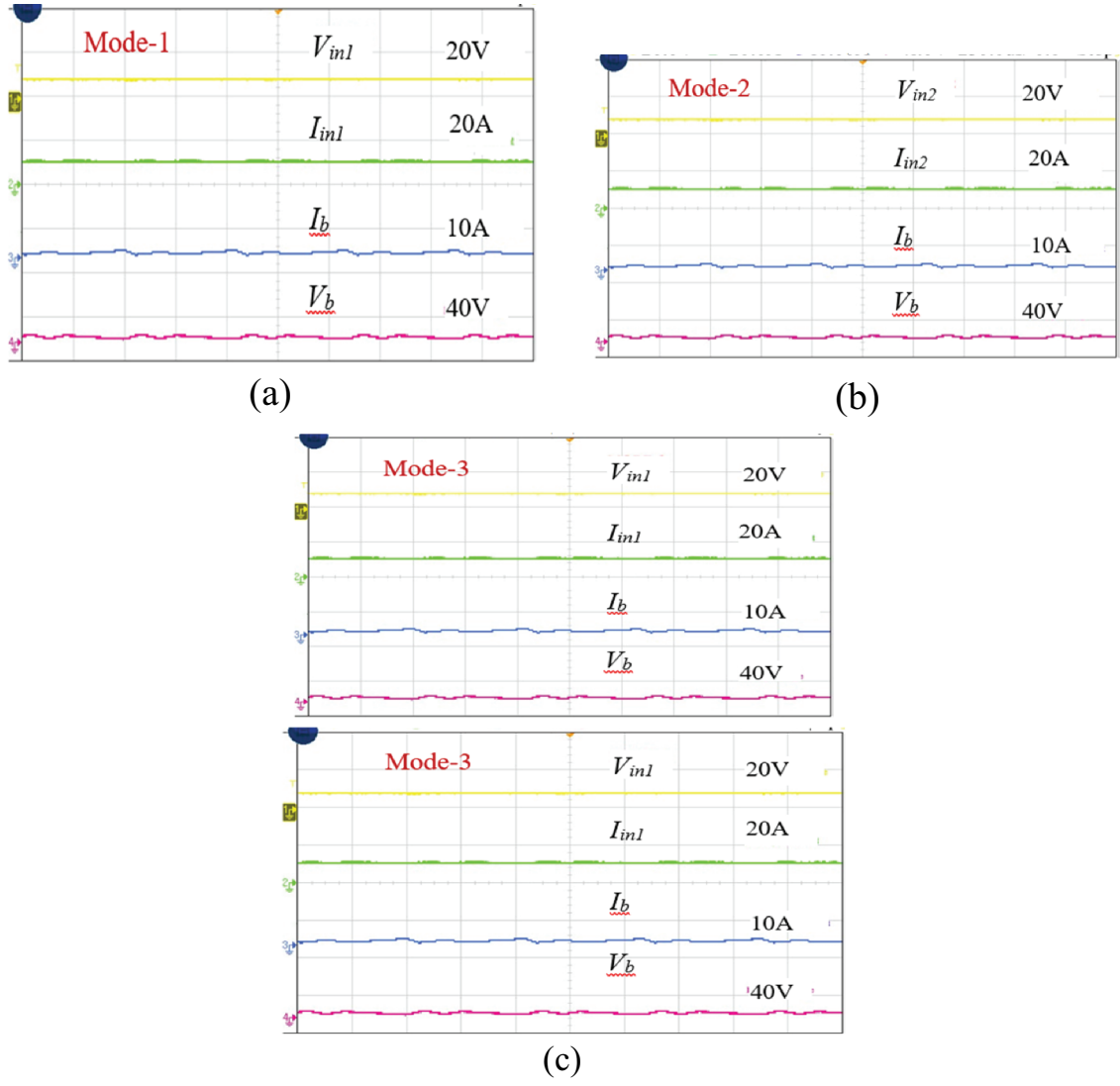

Figure 12. Experimental results, (a) mode-1 (power flow from grid (source) to EV battery (load)), (b) mode-2 (power flow from PV (source) to EV battery (load)), (c) mode-3 (power flow from both grid and PV (sources) to EV battery (load)).

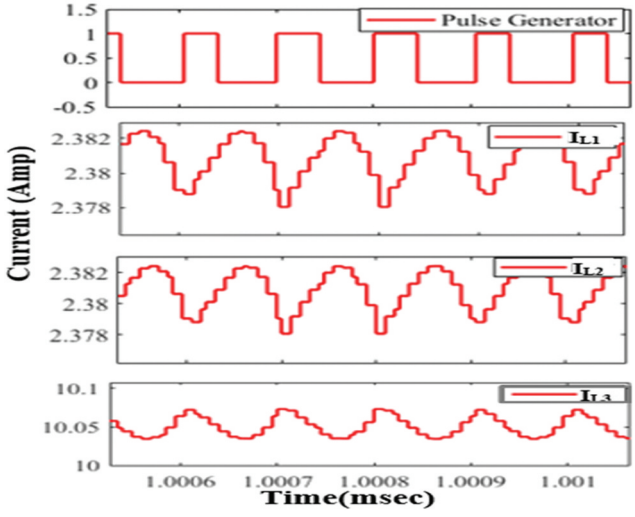

Figure 13. Current through inductor L_1, L_2, and L_3 during mode 1.

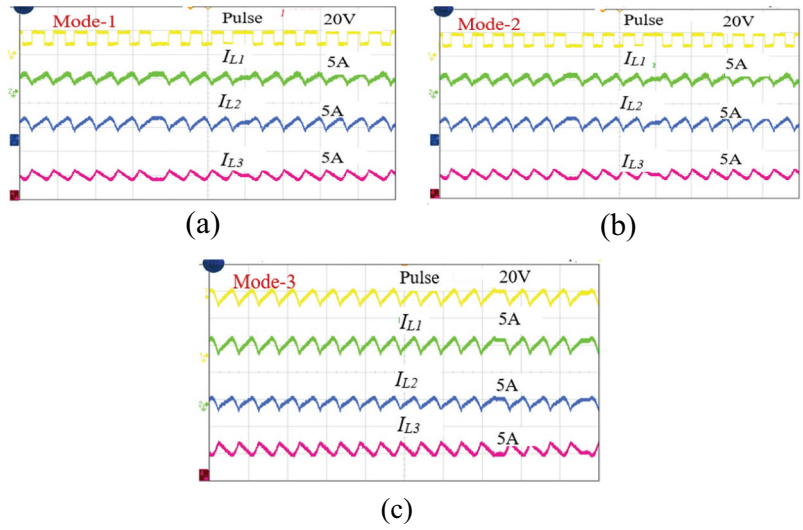

Figure 14. Experimental results for inductor currents, (a) mode-1 (pulse, inductor current), (b) mode-2 (pulse, inductor current), (c) mode-3 (inductor current).

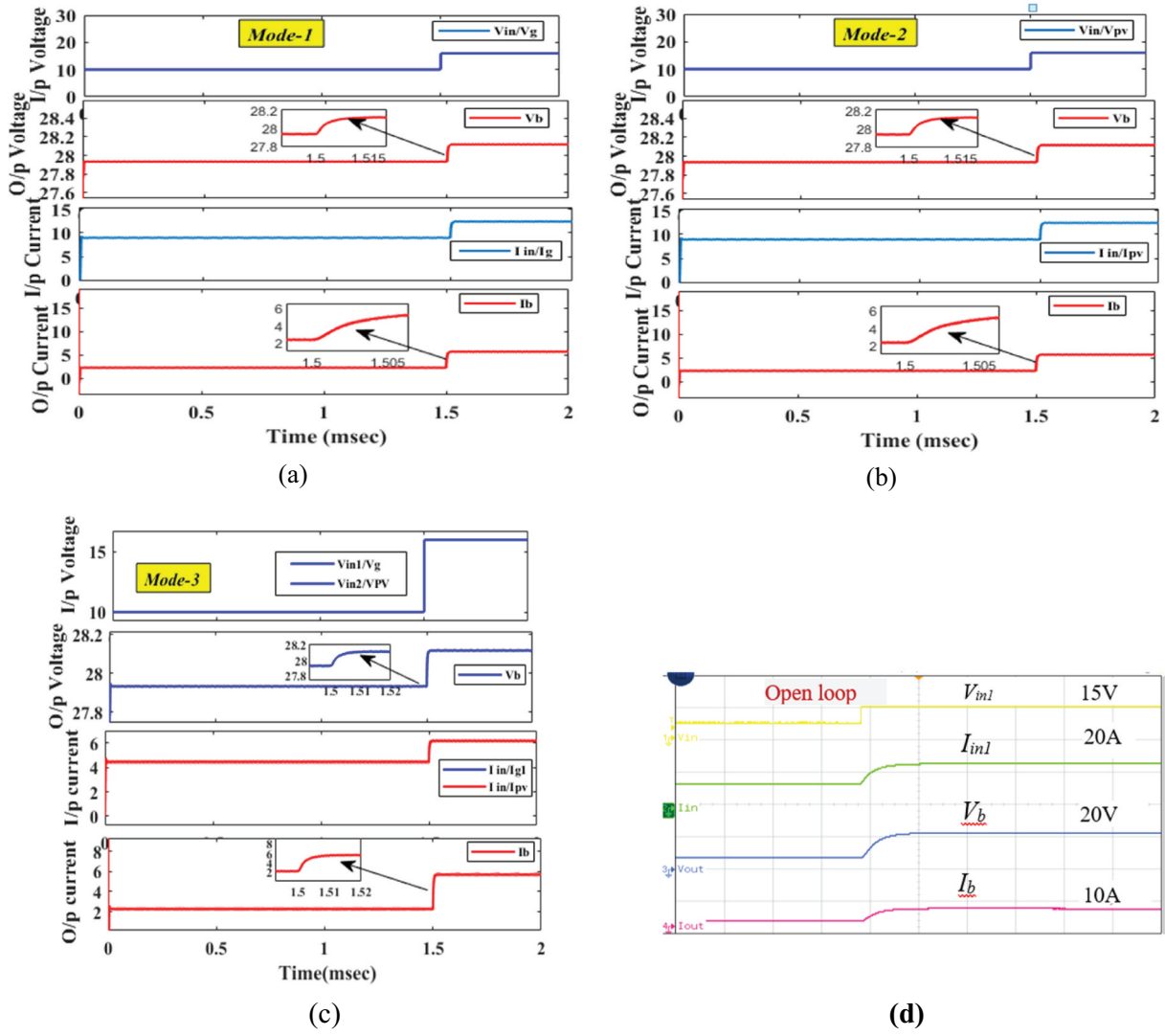

Figure 15. Simulation results of input voltages, input currents, output voltages, output currents during transient condition for, (a) mode-1, (b) mode-2, (c) mode-3, and (d) experimental results.

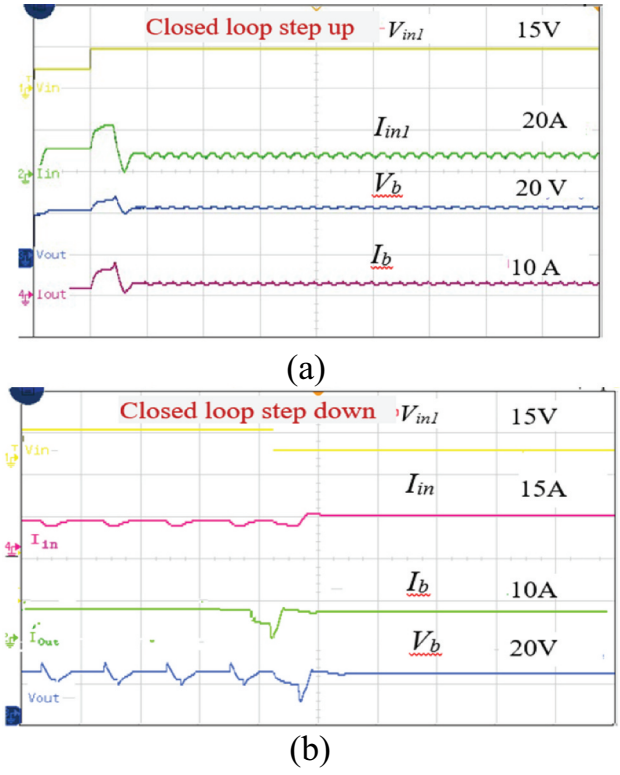

Figure 16. Experimental results of input voltages, input currents, battery current and voltage, (a) during step up input voltage condition (transient condition) with PI controller, (b) during step down input voltage condition (transient condition) with PI controller.

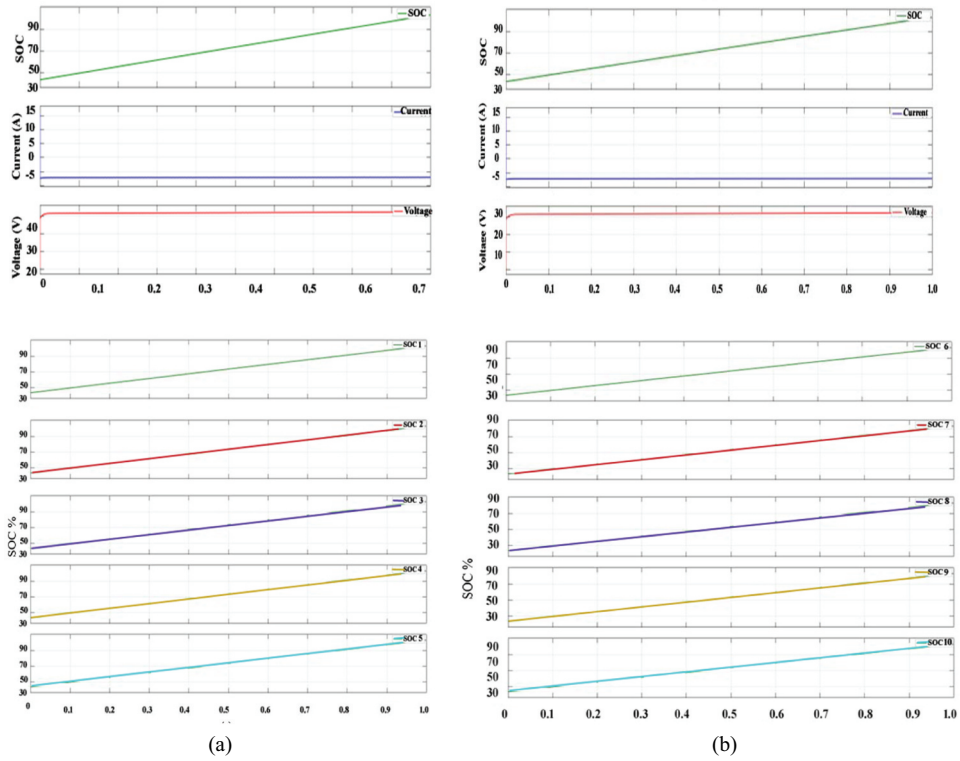

Figure 17. Charging status of EV batteries from 40% to 90% SOC, (a) sample of a single battery voltage, battery current and SOC, first set of five battery SOC for 48V vehicle batteries, and (b) sample of single battery voltage, battery current and SOC, second set of five battery SOC for 28V vehicle batteries.

the step down and step-up voltages as illustrated in Figure 16. EV battery charging controller controls the output voltage. Maintenance of constant output 28.2 V is achieved using the PI controller as shown in Figure 16. EV battery charging state, as shown in Figure 17(a,b), and the charging status of EV battery initially from 40% to 90% for 5 EV batteries at 28 V, and rest of 5 EV batteries at 48 V are depicted in Figure 17.

8. Conclusion

In this paper, a novel MSNQRC power electronics interface powered by a PV/Grid-EV battery system with the CC-CV controller has been analysed. First, the parametric design and selection of PV modules are discussed in relation to load demand. To demonstrate the capabilities of MSNQRC, various modes of operation have been discussed. From the analysis, it can be inferred that a PV hybrid system is suitable for EVCS (EV battery charge with a grid/PV station) to reduce the grid dependency. The converter parameters change due to the converter's ageing. Therefore, this paper, along with the design and analysis of MSNQRC, presents the reliability analysis of converter based on degradation with the computation of component failure rates. The study considers the impact of input voltage, duty cycle, output power, and gain on the converter's reliability, while operating in an open loop configuration. The experimental results (300W prototype) and simulation results have been used to confirm the MSNQRC's functionality.

Disclosure statement

No potential conflict of interest was reported by the author(s).

Notes on contributors

Harini S received the B.E. degree from Avinashilingam University, India, in 2010, and the M.E. degree in power electronics and drives from Anna University, in 2014. She is currently pursuing the Ph.D. degree from SRM Institute of Science and Technology, Kattankulathur, India, with a focus on design of power electronic converters for electric vehicle charging applications. Her research interests include design and control of power electronic converters, and renewable energy systems.

Chellammal N received her M.S. degree in Electrical Drives and Automation from Tashkent State Technical University, Tashkent, CIS (a former USSR) and her Ph.D. degree in Power Electronics from the Faculty of Engineering, SRM Institute of Science and Technology, Chennai, India. She is currently working as an Associate Professor at SRM Institute of Science and Technology. She has authored or co-authored more than 30 papers which are published in international journal including IEEE Access, Wiley, and IEEE international conferences etc. She is also serving as reviewer for many peer reviewed journals including IEEE transactions. Her research interests include modelling of power electronic converters and drives, EV charging, grid integration of renewable energy resources and design of controllers.

Ramesh C. Bansal has over 25 years of teaching, research, academic leadership, and industrial experience. Currently he is Professor in EE Dept. at the University of Sharjah, UAE and Extraordinary Professor at the University of Pretoria, South Africa. In previous postings, he was Professor and Group head (Power) at the University of Pretoria, and worked with University of Queensland, Australia; USP, Fiji; BITS Pilani, India. Prof. Bansal has published over 450 journal articles, conf. papers, books/book chapters. He has Google citations of over 20000 and h-index of 70. He has supervised 25 PhD and 5 Post Docs. Prof. Bansal has significant attracted significant funding from Industry and Government Organisations. He is an Editor of reputed journals including IEEE Systems Journal, EPCS, SGSE. He is a Fellow, and CP Engg IET-UK, Fellow IE (India), and Senior Member IEEE. He has diversified research interests in the areas of Renewable Energy, Power Systems and Smart Grid.

ORCID

Ramesh C Bansal http://orcid.org/0000-0002-1725-2648

References

[1] Feldman D, Barbose G, Margolis R, et al. Photovoltaic (PV) pricing trends: historical, recent, and near-term projections. NREL-DOE Tech Rep. 2012 November:1–30. doi: 10.2172/1059147

[2] García-Triviño P, Fernández-Ramírez LM, Torreglosa JP, et al. Control of electric vehicles fast charging station supplied by PV/energy storage system/grid. In: IEEE International Energy Conference (ENERGYCON); Leuven, Belgium; 2016. p. 1–6. doi: 10.1109/ENERGYCON.2016.7514120

[3] Bendjedia B, Rizoug N, Boukhnifer M, et al. Intelligent energy management of a multisource power supply for electric vehicle application. In: IEEE Vehicle Power and Propulsion Conference (VPPC); Belfort, France; 2017. p. 1–6. doi: 10.1109/VPPC.2017.8330922

[4] Bansal RC, Bhatti TS. Small signal analysis of isolated hybrid power systems: reactive power and frequency control analysis. Oxford, U.K: Alpha Science International; 2008. https://books.google.co.in/books?id=Qm5FyQEACAAJ

[5] Singh M, Thirugnanam K, Kumar P, et al. Real-time coordination of electric vehicles to support the grid at the distribution substation level. IEEE Syst J. 2015 Sept;9(3):1000–1010. doi: 10.1109/JSYST.2013.2280821.2280821

[6] Thirugnanam K, P ERJT, Singh M, et al. Mathematical modeling of Li-ion battery using genetic algorithm approach for V2G applications. IEEE Trans Energy Convers. 2014 June;29(2):332–343. doi: 10.1109/TEC.2014.2298460

[7] Das R, Thirugnanam K, Kumar P, et al. Mathematical modeling for economic evaluation of electric vehicle to smart grid interaction. IEEE Trans Smart Grid. 2014 March;5(2):712–721. doi: 10.1109/TSG.2013.2275979

[8] Thirugnanam K, Joy TPER, Singh M, et al. Modeling and control of contactless based smart charging station in V2G scenario. IEEE Trans Smart Grid. 2014 Jan;5(1):337–348. doi: 10.1109/TSG.2013.2272798

[9] Kalakanti AK, Rao S. Charging station planning for electric vehicles systems. Systems. 2022;10(1):6–26. doi: 10.3390/systems10010006

[10] Ahmad F, Iqbal A, Ashraf I. Optimal location of electric vehicle charging station and its impact on distribution network: a review. Energy Rep. 2022;8(2352–4847):2314–2333. doi: 10.1016/j.egyr.2022.01.180

[11] Mbungu NT, Ismail AA, ElNady AM, et al. Impact of electric vehicles on smart grid voltage/power under various loading conditions: a survey. Int J Model Simulat. 2023;43(6):1041–1057. doi: 10.1080/02286203.2022.2148180

[12] Danese A, Torsæter BN, Sumper A, et al. Planning of high-power charging stations for electric vehicles: a review. Appl Sci. 2022;12(7):3214. doi: 10.3390/app12073214

[13] He P, Khaligh A. Comprehensive analyses and comparison of 1 kW isolated DC–DC converters for bidirectional EV charging systems. IEEE Trans Transp Electrif. 2017 March;3(1):147–156. doi: 10.1109/TTE.2016.2630927

[14] Kerler M, Burda P, Baumann M, et al. A concept of a high-energy, low-voltage EV battery pack. In: IEEE International Electric Vehicle Conference (IEVC); Florence, Italy; 2014. p. 1–8. doi: 10.1109/IEVC.2014.7056185

[15] Musavi F, Edington M, Eberle W, et al. Evaluation and efficiency comparison of front end AC DC plug-in hybrid charger topologies. IEEE Trans Smart Grid. 2012 March;3(1):413–421. doi: 10.1109/TSG.2011.2166413

[16] Choe G-Y, Kim J-S, Lee B-K, et al. A Bi-directional battery charger for electric vehicles using photovoltaic PCS systems. In: IEEE Vehicle Power and Propulsion Conference; Lille, France; 2010. p. 1–6. doi: 10.1109/VPPC.2010.5729223

[17] Patil D, McDonough MK, Miller JM, et al. Wireless power transfer for vehicular applications: overview and challenges. IEEE Trans Transp Electrif. 2018 March;4(1):3–37. doi: 10.1109/TTE.2017.2780627

[18] Nasir A. Design and development of a constant Current constant voltage fast battery charger for electric vehicles. In: 4th International Conference on Modern Research in Science, Engineering and Technology; 2021. p. 13–55. doi: 10.33422/4th.msetconf.2021.03.02

[19] Wang S, Liu Y, Wang X. Resonant converter for battery charging applications with CC/CV output profiles. IEEE Access. 2020;8:54879–54886. doi: 10.1109/ACCESS.2020.2981595

[20] Tar B, Fayed A. An overview of the fundamentals of battery chargers. In: IEEE 59th International Midwest Symposium on Circuits and Systems (MWSCAS); Abu Dhabi, United Arab Emirates; 2016. p. 1–4. doi: 10.1109/MWSCAS.2016.7870048

[21] Madhumitha R, Priya P, Saravanan S. Hybrid renewable energy based electric vehicles charging station. In: 2nd International Conference on Advance Computing and Innovative Technologies in Engineering (ICACITE), Greater; Noida, India; 2022. p. 2348–2352. doi: 10.1109/ICACITE53722.2022.9823451

[22] Kumar V, Teja VR, Singh M, et al. PV based off-grid charging station for electric vehicle, IFAC-Papers on line. 2019;52(4):276–281. doi: 10.1016/j.ifacol.2019.08.211

[23] Chandra Mouli GR, Bauer P, Zeman M. System design for a solar powered electric vehicle charging station for workplaces. Appl Energy. 2016;168(306–2619):434–443. doi: 10.1016/j.apenergy.2016.01.110

[24] Kumar S, Upadhyay T, Gupta OH. Power quality improvement and signal conditioning of pv array and grid interfaced off-board charger for electric vehicles with V2G and G2V capabilities. Chin J Electr Eng. 2023 December;9(4):132–143. doi: 10.23919/C023.000027

[25] Tarzamni H, Tahami F, Fotuhi-Firuzabad M, et al. Reliability analysis of buck-boost converter considering the effects of operational factors, 10th Int Power Electron Drive Syst Technol Conf PEDSTC. 2019. pp. 647–652. doi: 10.1109/PEDSTC.2019.8697266

[26] Adefarati T, Bansal RC. Reliability, economic and environmental analysis of a microgrid system in the presence of renewable energy resources. Appl Energy. 2018 August;236:1089–1114. doi: 10.1016/j.apenergy.2018.12.050

[27] Chiodo E, Lauria D. Some basic properties of the failure rate of redundant reliability systems in industrial electronics applications. IEEE Trans Ind Electron. 2015;62(8):5055–5062. doi: 10.1109/TIE.2015.2404306

[28] Yang S, Bryant A, Mawby P, et al. An industry-based survey of reliability in power electronic converters. IEEE Trans Ind Appl. 2011;47(3):1441–1451. doi: 10.1109/TIA.20112124436

[29] Liu Y, Huang M, Wang H, et al. Reliability-oriented optimization of the LC filter in a buck DC-DC converter. IEEE Trans Power Electron. 2017;32(8):6323–6337. doi: 10.1109/TPEL.2016.2619690

[30] Rahimi T, Hosseini SH, Sabahi M, et al. Three-phase soft-switching-based interleaved boost converter with high reliability. IET Power Electron. 2017;10(3):377–386. doi: 10.1049/iet-pel.2016.0211

[31] Aghdam FH, Abapour M. Reliability and cost analysis of multistage boost converters connected to PV panels. IEEE J Photovoltaics. 2016;6(4):981–989. doi: 10.1109/JPHOTOV.2016.2566.8852.5668.85

[32] Khosroshahi A, Abapour M, Sabahi M. Reliability evaluation of conventional and interleaved DC-DC boost converters. IEEE Trans Power Electron. 2015;30(10):5821–5828. doi: 10.1109/TPEL.2014.2380829

[33] Zhou D, Wang H, Blaabjerg F. Mission profile based system-level reliability analysis of Dc/Dc converters for a backup power application. IEEE Trans Power Electron. 2018;33(9):8030–8039. doi: 10.1109/TPEL.2017.2769161

[34] United States Dept of Defense. Military Handbook: Reliability Prediction of Electronic Equipment.MIL-HDBK-217F. Arlington, VA, USA: Department of Defence; 1991.